

Correlation between electronic structure and emergence of superconductivity in $\text{Bi}_{2-x}\text{Sb}_x\text{Te}_{3-y}\text{Se}_y$ ($y \sim 1.2$) studied by x-ray emission spectroscopy and density functional theory

Hitoshi Yamaoka ^{1,*} Harald O. Jeschke ² Huan Li ^{2,†} Tong He ^{2,‡} Naohito Tsujii ³
 Nozomu Hiraoka ⁴ Hirofumi Ishii ⁴ Hidenori Goto ² and Yoshihiro Kubozono ²

¹RIKEN Spring-8 Center, Sayo, Hyogo 679-5148, Japan

²Research Institute for Interdisciplinary Science, Okayama University, Okayama 700-8530, Japan

³International Center for Materials Nanoarchitectonics, National Institute for Materials Science, Sengen 1-2-1, Tsukuba, 305-0047, Japan

⁴National Synchrotron Radiation Research Center, Hsinchu 30076, Taiwan



(Received 6 March 2023; revised 7 May 2023; accepted 20 June 2023; published 25 July 2023)

Chemical composition and pressure dependencies of the electronic structures of $\text{Bi}_{2-x}\text{Sb}_x\text{Te}_{3-y}\text{Se}_y$ ($y \sim 1.2$) have been studied by the high-resolution x-ray absorption spectroscopy. We find a shift of the Bi- L_3 absorption edge due to Sb substitution, suggesting a change in the Bi charge state. In the pressure dependence, the electronic structures of $\text{Bi}_2\text{Te}_2\text{Se}$ and $\text{Bi}_{1.5}\text{Sb}_{0.5}\text{Te}_2\text{Se}$ start to change below the pressure of the first structural phase transition where the emergence of the superconductivity was observed and then show a large change just around that pressure. This is in contrast to the behavior observed in Bi_2Se_3 -based compounds where the structural phase transition was necessary for the onset of superconductivity. We performed density functional theory calculations using the experimentally determined structures for $\text{Bi}_2\text{Te}_2\text{Se}$ and $\text{Bi}_{1.5}\text{Sb}_{0.5}\text{Te}_2\text{Se}$. We show that both compounds become metallic within the rhombohedral phase below the pressure of the first structural transition and we thus corroborate the experimental observation. The experimental and calculated results show that closing the gap and increasing the density of states in the rhombohedral phase are the triggers to induce superconductivity.

DOI: [10.1103/PhysRevB.108.035146](https://doi.org/10.1103/PhysRevB.108.035146)

I. INTRODUCTION

Two-dimensional topological insulators show conducting edge states. Three-dimensional (3D) topological insulators are characterized by an insulating bulk state and gapless surface states with a Dirac cone showing a helical spin structure in momentum space [1]. A_2B_3 ($A = \text{Bi}, \text{Sb}; B = \text{S}, \text{Se}, \text{Te}$) series have been considered to be candidates for 3D topological insulators, but they are not good insulators in the bulk because of natural defects and the resulting carrier doping. As an alternative, the quaternary family $\text{Bi}_{2-x}\text{Sb}_x\text{Te}_{3-y}\text{Se}_y$ is a promising candidate to study 3D topological insulators where bulk carrier numbers are negligible [2]. In these materials, the chalcogens (Te and Se) are separated into different lattice sites, forming ordered Te-Bi-Se-Bi-Te quintuple layers and reducing defect formation.

Another great advantage of $\text{Bi}_{2-x}\text{Sb}_x\text{Te}_{3-y}\text{Se}_y$ is that the Fermi level and the Dirac cones can be controlled by changing the chemical substitution parameters of x and y . Angle-resolved photoelectron spectroscopy (ARPES) revealed that the chemical potential was kept to be in the bulk band gap, whereas the Dirac cone dispersion changed systematically and the Dirac point moved up in energy with increasing x , chang-

ing the sign of the Dirac carriers from n type to p type at $x \sim 0.9$ [3]. These materials show bulk superconductivity under pressure [4]. In Bi_2Se_3 -based compounds, the first structural phase transition where the electronic structure also changes significantly is a trigger of the emergence of superconductivity under pressure [5,6]. In contrast, in $\text{Bi}_{2-x}\text{Sb}_x\text{Te}_{3-y}\text{Se}_y$ ($y \sim 1.2$) pressure-induced bulk superconductivity was observed at a pressure below the first phase transition [4]. Density functional theory (DFT) calculations of $\text{Bi}_{1.5}\text{Sb}_{0.5}\text{Te}_{1.5}\text{Se}_{1.5}$ showed the closing of the band gap at 5.8 GPa [7]. Therefore, we should expect changes in the electronic structure below the pressure of the first phase transition in $\text{Bi}_{2-x}\text{Sb}_x\text{Te}_{3-y}\text{Se}_y$. On the other hand, in $\text{Bi}_{2-x}\text{Sb}_x\text{Te}_{3-y}\text{Se}_y$ ($x = 1.0, y = 2.0$) the emergence of superconductivity was recently found around the pressure of the first structural transition (P_{s1}) [8]. This difference was considered to be due to the Te amount in these systems. In $\text{Bi}_{2-x}\text{Sb}_x\text{Te}_{3-y}\text{Se}_y$ the chemical composition and pressure dependencies of the relation between the electronic structure and T_c may be the key to understanding these phenomena, but there are no reports of the electronic structure, especially for the measurement under pressure so far.

In this paper, we conduct a systematic study of the electronic structures of $\text{Bi}_{2-x}\text{Sb}_x\text{Te}_{3-y}\text{Se}_y$ ($y \sim 1.2$). We measured the chemical composition (x) and pressure dependencies of the high-resolution x-ray absorption spectra with partial fluorescence yield mode (PFY-XAS) at the Se- K and Bi- L_3 absorption edges [9–11]. We measured the electronic structures of the key elements of Bi and Se separately. Our XAS study is intrinsically bulk sensitive and thus cannot discuss surface states or surface topology; instead, we study the correlation between bulk electronic structure and

*Corresponding author: yamaoka@spring8.or.jp

†Present address: SUSTech Energy Institute for Carbon Neutrality, Department of Mechanical and Energy Engineering, Southern University of Science and Technology, Shenzhen, 518055, China.

‡Present address: School of Chemistry and Chemical Engineering, Shaanxi Normal University, Xi'an, Shaanxi 710062, China.

superconductivity. The purpose of this paper is to clarify the chemical composition and pressure dependence of the correlation between the electronic structure and the emergence of superconductivity. The chemical composition dependence of the XAS spectra may give another perspective on the electronic structure compared to ARPES. We find an energy shift of the Bi- L_3 absorption edge between $x = 0$ and 1.0. Pressure starts to change the electronic structure below P_{s1} , which may correlate with the emergence of superconductivity within the rhombohedral phase. We also performed fully relativistic DFT calculations, which account for the effects of spin-orbit coupling for $\text{Bi}_2\text{Te}_2\text{Se}$ and $\text{Bi}_{1.5}\text{Sb}_{0.5}\text{Te}_2\text{Se}$. We can show how the observed increase in the superconducting transition temperature is related to the density of states (DOS) at the Fermi level, and we find a metallization in both compounds below P_{s1} .

II. METHODS

A. Experiments

Single crystals of $\text{Bi}_{2-x}\text{Sb}_x\text{Te}_{3-y}\text{Se}_y$ ($\text{Bi}_{2.1}\text{Te}_{1.8}\text{Se}_{1.2}$, $\text{Bi}_{1.75}\text{Sb}_{0.25}\text{Te}_{1.89}\text{Se}_{1.11}$, $\text{Bi}_{1.5}\text{Sb}_{0.5}\text{Te}_{1.68}\text{Se}_{1.32}$, and $\text{Bi}_{1.09}\text{Sb}_{0.91}\text{Te}_{1.81}\text{Se}_{1.19}$) were prepared with Bi, Bi_2O_3 , and Bi_2Se_3 for comparison [4]. Crystals of $\text{Bi}_{2-x}\text{Sb}_x\text{Te}_{3-y}\text{Se}_y$ were grown by a conventional melt-growth method using stoichiometric amounts of Bi, Sb, Te, and Se powders [4]. The powders were sealed in a quartz tube, which was heated at 850 °C for 24 hours, then slowly cooled down to 550 °C at a rate of 6 °C/h, and then quenched with ice water. The energy-dispersive x-ray spectroscopy (EDX) spectrum of the crystals was recorded with an EDX spectrometer equipped with a scanning electron microscope (KEYENCE VE-9800-EDAX Genesis XM2). The EDX spectra were measured for 5–10 different positions at room temperature.

The PFY-XAS spectra were measured at BL12XU, SPring-8 [12,13]. Johann-type spectrometers were equipped with a spherically bent Si(577) analyzer of a radius of ~ 1 m for Se $K\beta_1$ emission and Si(555) for Bi $L\alpha_1$ emission with a Si solid-state detector (Amptech). We analyze the two emission lines of the $K\beta$ at the Se- K absorption edge and the $L\alpha$ at the Bi- L_3 absorption edge [6,14]. At the emitted photon energy of 12.66 keV the overall energy resolution was set to be 1.5 eV. It is noted that one can discuss the relative change in the energy on the order of 0.1 eV, which is one order of magnitude smaller than the energy spread of the analyzer. The intensities of the measured spectra were normalized using the intensity of the incident beam that was monitored just before the sample. The errors in the intensity and energy of each component of the PFY-XAS spectrum arose mainly from the statistical errors of the total counts and the fit errors. The intensities of the PFY-XAS spectra are normalized by the areas in the measured-energy range.

The incident beam energy was corrected using the absorption edges of Au L_2 and L_3 in every experiment. However, there are shifts of the incident energies of the PFY-XAS spectra at the Se- K and Bi L_3 edges between the samples of $x = 0.5$ and 0 (Figs. 3 and 4), which were measured as different series of experiments. Here, we did not correct these incident energies because we only discuss the relative change in the energy.

We also measured the PFY-XAS spectra at the Bi- L_2 absorption edge using the emission of Bi $L\beta_1$ ($3d_{3/2}-2p_{1/2}$) with an analyzer crystal of Si(880) to compare with the spectra at the Bi- L_3 absorption edge. We normalize the continuum fluorescence part of the spectrum at the L_2 absorption edge to be half the value of that at the L_3 absorption edge [15].

For the high-pressure experiments in the x-ray emission spectroscopy, the x-ray beam was focused to ~ 30 (horizontal) $\times \sim 20$ (vertical) μm^2 at the sample position using a toroidal and a Kirkpatrick-Baez mirror. High-pressure conditions were achieved using a diamond anvil cell coupled with a gas membrane. A Be-gasket of 3 mm in diameter and approximately 100 μm thick was pre-indented to approximately 40–50 μm thickness around the center. The diameter of the sample chamber in the gasket was approximately 120 μm and the diamond anvil culet size was 300 μm . A pressure medium of Daphne 7474 was used for the DAC. Pressure was monitored by the ruby fluorescence method [16–18]. All measurements here were performed at room temperature.

B. Theoretical calculations

We performed scalar and fully relativistic electronic structure calculations for $\text{Bi}_2\text{Te}_2\text{Se}$ and $\text{Bi}_{1.5}\text{Sb}_{0.5}\text{Te}_2\text{Se}$ with the full potential local orbital (FPLO) basis set [19] and the GGA exchange correlation functional [20]. We use the experimentally determined structures under pressure. We first interpolated the lattice parameters in order to avoid spurious noise in the crystal structures, and we sampled the structures in 0.5 GPa pressure steps. For these structures (65 in the case of $\text{Bi}_2\text{Te}_2\text{Se}$ and 84 in the case of $\text{Bi}_{1.5}\text{Sb}_{0.5}\text{Te}_2\text{Se}$), we fully optimized all internal Wyckoff positions for fixed symmetry and lattice parameters using GGA calculations. We extract the electronic structure at the GGA + SO level using $24 \times 24 \times 24$ k points.

III. RESULTS

A. Chemical composition dependence

We measured the x dependence of the PFY-XAS spectra of $\text{Bi}_{2-x}\text{Sb}_x\text{Te}_{3-y}\text{Se}_y$ ($x = 0, 0.25, 0.5, 0.91$, and $y \sim 1.2$) with the reference samples of Bi, Bi_2O_3 , and Bi_2Se_3 at the Se- K and Bi- L_3 absorption edges. The intensity is normalized by the integrated area in the measured energy range. Figures 1(a) and 1(b) show the PFY-XAS spectra of $\text{Bi}_{2-x}\text{Sb}_x\text{Te}_{3-y}\text{Se}_y$ and Bi_2Se_3 at the Se- K absorption edge and ambient pressure. The main peaks around the absorption edge are labeled as A , B , and C . The absorption spectra at the Se- K absorption edge do not show a significant change when Sb is substituted for the Bi site. The absorption edge also does not change within the experimental errors. The results indicate that the Sb substitution does not affect the electronic structure of Se significantly, but that it affects the electronic structure of Bi because of the energy shift of the absorption edge as described below. The energies of the Se- K absorption edge of $\text{Bi}_{2-x}\text{Sb}_x\text{Te}_{3-y}\text{Se}_y$ are much higher than that of Bi_2Se_3 , indicating that the charge state of Se is higher than 3+ in $\text{Bi}_{2-x}\text{Sb}_x\text{Te}_{3-y}\text{Se}_y$. The intensity of the peak A of Bi_2Se_3 is much smaller than that of $\text{Bi}_{2-x}\text{Sb}_x\text{Te}_{3-y}\text{Se}_y$, while its width is larger. The peak position of the peak A in $\text{Bi}_{2-x}\text{Sb}_x\text{Te}_{3-y}\text{Se}_y$ is slightly higher than that

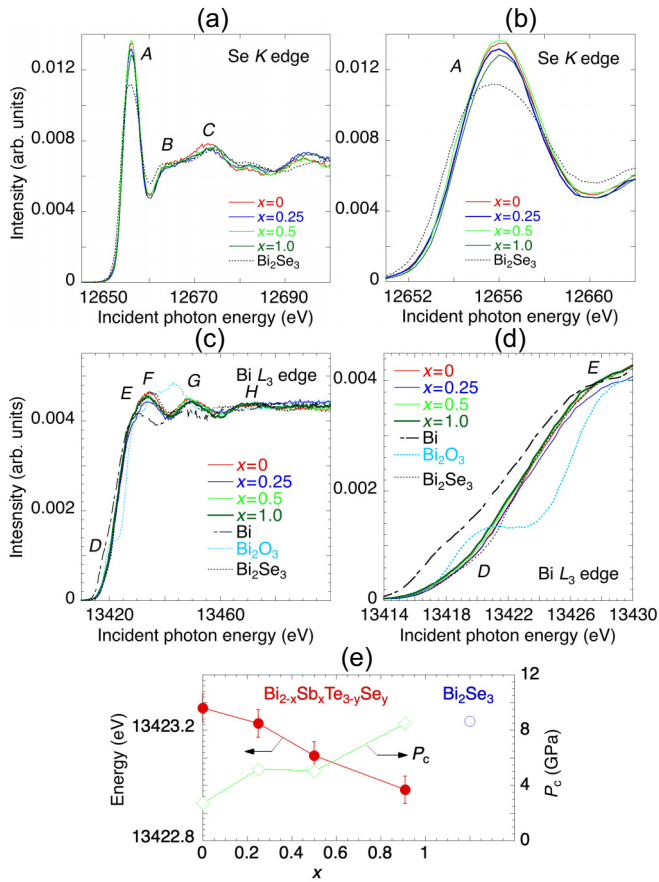


FIG. 1. (a) PFY-XAS spectra of $\text{Bi}_{2-x}\text{Sb}_x\text{Te}_{3-y}\text{Se}_y$ ($x = 0, 0.25, 0.5, 1.0$, and $y \sim 1.2$) and Bi_2Se_3 at the Se-K absorption edge. (b) Expanded views of the PFY-XAS spectra in (a) around the Se-K absorption edge. (c) PFY-XAS spectra of $\text{Bi}_{2-x}\text{Sb}_x\text{Te}_{3-y}\text{Se}_y$, Bi, Bi_2O_3 , and Bi_2Se_3 at the Bi-L₃ absorption edge. (d) Expanded views of the PFY-XAS spectra in (c) around the Bi-L₃ absorption edge. (e) Energy of the Bi-L₃ absorption edge of $\text{Bi}_{2-x}\text{Sb}_x\text{Te}_{3-y}\text{Se}_y$ (closed circles) and Bi_2Se_3 (open circles). In (e) the critical pressures for creating superconductivity in $\text{Bi}_{2-x}\text{Sb}_x\text{Te}_{3-y}\text{Se}_y$ (open diamonds) are also shown [4].

in Bi_2Se_3 . These results suggest more unoccupied states of Se 4*p* DOS and a larger band gap in $\text{Bi}_{2-x}\text{Sb}_x\text{Te}_{3-y}\text{Se}_y$ compared to the case of Bi_2Se_3 .

Figures 1(c) and 1(d) show the PFY-XAS spectra of $\text{Bi}_{2-x}\text{Sb}_x\text{Te}_{3-y}\text{Se}_y$, Bi, Bi_2O_3 , and Bi_2Se_3 at the Bi-L₃ absorption edge and ambient pressure. The main peaks around the absorption edge are labeled as D, E, F, G, and H. The energy of the absorption edge of $\text{Bi}_{2-x}\text{Sb}_x\text{Te}_{3-y}\text{Se}_y$ around 13 420 eV is near that of Bi_2Se_3 and higher than that of Bi_2O_3 , indicating that the Bi charge state is slightly higher than 3+. Here, we made spline fits for the XAS spectra and defined the energy of the absorption edge as the maximum of the second derivative curve.

The absorption edge energy normally corresponds to the Fermi level in metals. In $\text{Bi}_{2-x}\text{Sb}_x\text{Te}_{3-y}\text{Se}_y$ there is a band gap at ambient pressure and the Fermi level is located in the band gap [3]. In this case, the change in the energy position of the absorption edge is considered to reflect mainly changes in the energies of the conduction band, the valence band, the size of

the band gap or changes in the Bi charge state. The energy of the Bi-L₃ absorption edge decreases by approximately 0.3 eV when the Sb content x increases from 0 to 1 as shown in Fig. 1(e), while the energy of the Se-K absorption edge did not show a significant x dependence [21]. On the other hand, ARPES showed that Sb substitution raised the Dirac point and the energy of the valence band, and finally a slight increase of the band gap defined as the energy difference between the conduction and the valence bands [3]. The shift of the energy of the Bi-L₃ absorption edge to the lower-incident energy side seems to show a decrease in the energy of the conduction band with the Sb substitution and a decrease in the band gap. However, ARPES and the resistivity measurements showed rather the increase in the band gap with the Sb substitution as described above [2,3]. A possible explanation of the downward shift of the energy of the Bi-L₃ absorption edge is due to the decrease of the Bi charge states with the Sb substitution. This may result in the decrease of the relative energy of the Fermi level to the energy of the valence band, and in the increase of the band gap as observed in ARPES.

In Fig. 1(e) we also show the onset pressures for creating superconductivity [4]. P_c increases with x . The bulk band gap shows an increasing trend with x [3]. Our DFT calculations, using the experimentally determined structures described below, indicate a wider band gap of 0.25 eV at ambient pressure in $\text{Bi}_{1.5}\text{Sb}_{0.5}\text{Te}_2\text{Se}$ compared to an extrapolated one of 0.20 eV in $\text{Bi}_2\text{Te}_2\text{Se}$. This suggests that the critical pressure to produce superconductivity increases with the Sb substitution. Generally, DOS at the Fermi level and thus closing the band gap is necessary for the appearance of the superconducting state. Pressure can change the bandwidth and as a consequence the band gap. Therefore, a higher pressure may be required for creating superconductivity in the case of a wider band gap.

B. Pressure dependence of the XAS spectra:

$\text{Bi}_{1.5}\text{Sb}_{0.5}\text{Te}_{1.68}\text{Se}_{1.32}$

We measured the pressure dependence of the PFY-XAS spectra for the $x = 0.5$ and 0 samples ($\text{Bi}_{1.5}\text{Sb}_{0.5}\text{Te}_{1.68}\text{Se}_{1.32}$ and $\text{Bi}_{2.1}\text{Te}_{1.8}\text{Se}_{1.2}$) at both the Se-K and Bi-L₃ absorption edges. Under pressure, both samples have the phases I ($R\bar{3}m$), II ($C2/m$), and III (9/10-fold $C2/m$) with different crystal structures of rhombohedral, monoclinic, and another monoclinic structure, respectively [4,21]. Figures 2(a)–2(c) show the PFY-XAS spectra of the $x = 0.5$ sample at the Se-K absorption edge. In Figs. 2(d) and 2(g) we show examples of the fits to the PFY-XAS spectra at 4.1 GPa. Figures 2(e) and 2(f) show the PFY-XAS spectra at the Bi-L₃ absorption edge.

In the fits, we assumed some Voigt functions with an arctan-like fluorescence background for simplicity [6]. From the analogy to the spectra of selenium compounds [22–26], the peak A is attributed to a $1s-4p$ dipole transition and to Se 4*d* partial density of states hybridized with the Bi 6*s* and 6*p* states. The peak B is due to multiple scattering sensitive to the local structure around Se and the partial density of states of Se 4*d* character in the continuum. We assumed five components of the peaks D, E, F, G, and H near the Bi-L₃ absorption edge [27–29]. The peak D is assigned as a dipole-allowed transition of a $2p_{3/2}$ electron into 6*s* states [26,28,30,31]. A weak intensity of the peak D [see also Fig. 3(e)] suggests

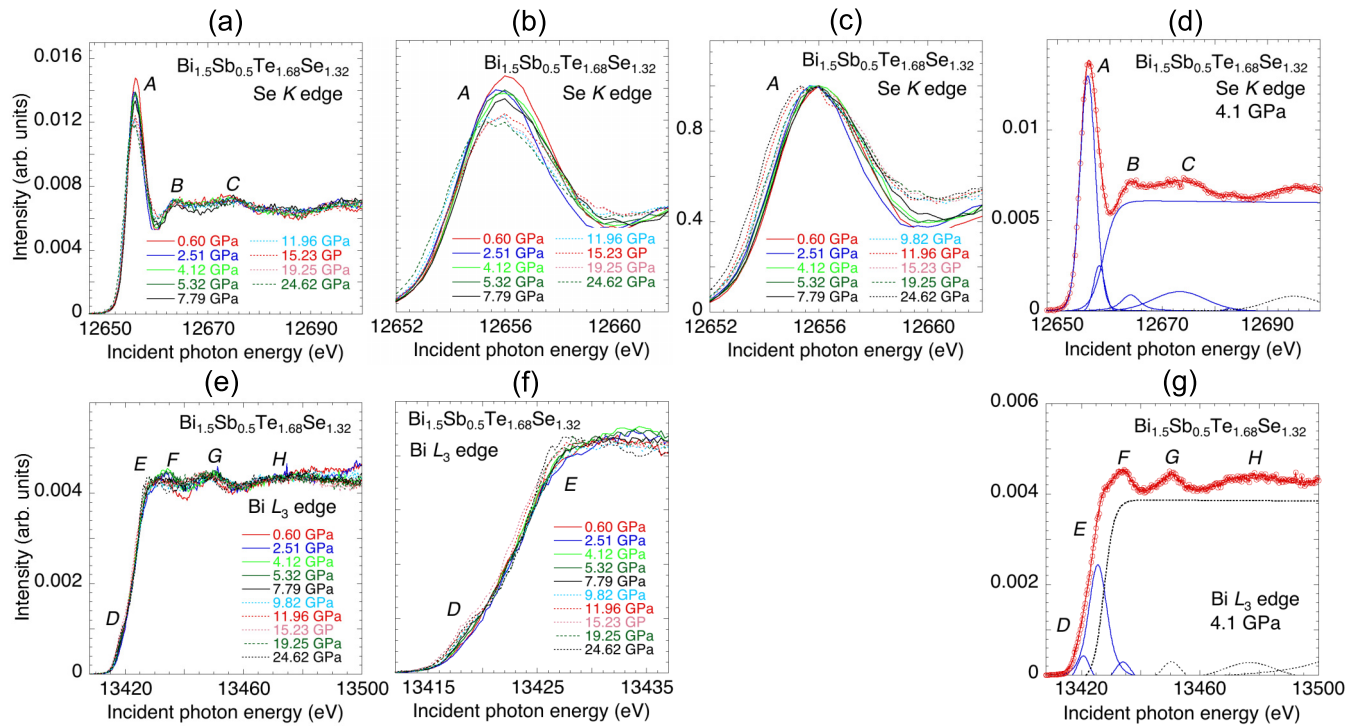


FIG. 2. Absorption spectra of $\text{Bi}_{1.5}\text{Sb}_{0.5}\text{Te}_{1.68}\text{Se}_{1.32}$. (a) Pressure dependence of the PFY-XAS spectra at the Se-K absorption edge. (b) Expanded views of the PFY-XAS spectra in (a) around the Se K-absorption edge. (c) Expanded views of the PFY-XAS spectra in (a) around the Se K-absorption edge, where the intensity is normalized to the peak. (d) A fit example of the PFY-XAS spectrum at the Se-K absorption edge and 4.1 GPa. The main peaks around the absorption edge are labeled as A, B, and C. The open circles are the measured data. (e) Pressure dependence of the PFY-XAS spectra at the Bi-L₃ absorption edge. (f) Expanded views of the PFY-XAS spectra in (e) around the Bi-L₃ absorption edge. (g) A fit example of the PFY-XAS spectrum at the Bi-L₃ absorption edge and 4.1 GPa. The main peaks around the absorption edge are labeled as D, E, F, G, and H. The open circles are the measured data.

that the Bi 6s state is not filled completely. The increase in the intensity of the peak D with pressure may correspond to the increase in the hybridization [6,27]. Peaks E and F correspond to the transition of a $2p_{3/2}$ electron to $6d t_{2g}$ and e_g states [26].

In the $x = 0.5$ sample, superconductivity appears above 5 GPa and below T_c and increases rapidly around P_{s1} of 10–12 GPa as shown in Fig. 3 as a dense grey area. Figure 3(a) shows that the energy of the Se-K absorption edge starts to decrease gradually at a pressure below P_{s1} . A gradual decrease in the intensity of the peak A (Se 4p band) also occurs at a pressure below P_{s1} as shown in Fig. 3(b). The energy of the peak A does not change much around this pressure range, while the width of the peak A becomes broad and the Se-K absorption edge decreases with pressure. A sudden decrease in the intensities of the peaks A and B around 0.6–2.5 GPa in Figs. 3(b) and 3(c) are observed, although the origin is not known. The intensity and energy of the peak B are insensitive around the pressure of the structural transition from phase I to II, while the intensity of this peak decreased rapidly around the structural transition from phase II to III, as shown in Fig. 3(c).

The energy of the Bi-L₃ absorption edge starts to decrease below P_{s1} and decreases rapidly beyond P_{s1} as shown in Fig. 3(d). In this figure, we also show the energy where the intensity of the peak D (Bi 6s band) is 0.001, which follows the trend of the energy of the Bi-L₃ absorption edge. The

energy of the peak D gradually decreases from 5 to 10 GPa below P_{s1} as shown in Fig. 3(e). Thus, the energy of the Bi-L₃ absorption edge, the energy at which the intensity of the peak D is 0.001, and the energy of the peak D show similar pressure dependence. The intensity of the peak D increases rapidly around P_{s1} from phase I to II, while almost no change is observed around the transition from phase II to III, as shown in Fig. 3(e). The results indicate a pressure-induced increase of the unoccupied states of the Bi 6s band above P_{s1} . Figure 3(f) shows that both the intensity of the peak E (Bi 6d t_{2g} band) has a trend to increase with pressure with a small step-like increase around P_{s1} , while the energy of that does not show a clear pressure dependence related to the structural phase transitions or superconductivity. The increase in the intensity of the peak E indicates an increase in the unoccupied states of the Bi 6d band. Thus, the unoccupied states of both the Bi 6s and 6d bands increase with pressure, suggesting the increase of the hybridization. Figure 3(g) indicates that the intensity of peak F does not show pressure dependence. The energy of peak F decreases rapidly around the pressure where the superconductivity appears.

Both the Se-K and Bi-L₃ absorption edges shift to lower incident energies, indicating an increase of the unoccupied states above the Fermi level. The energy shift of the peak D is on the order of 1 eV between 0 and 10 GPa, while that of the Se-K absorption edge is on the order of 0.5 eV. The rapid increase in T_c around 10–12 GPa may be closely related to the

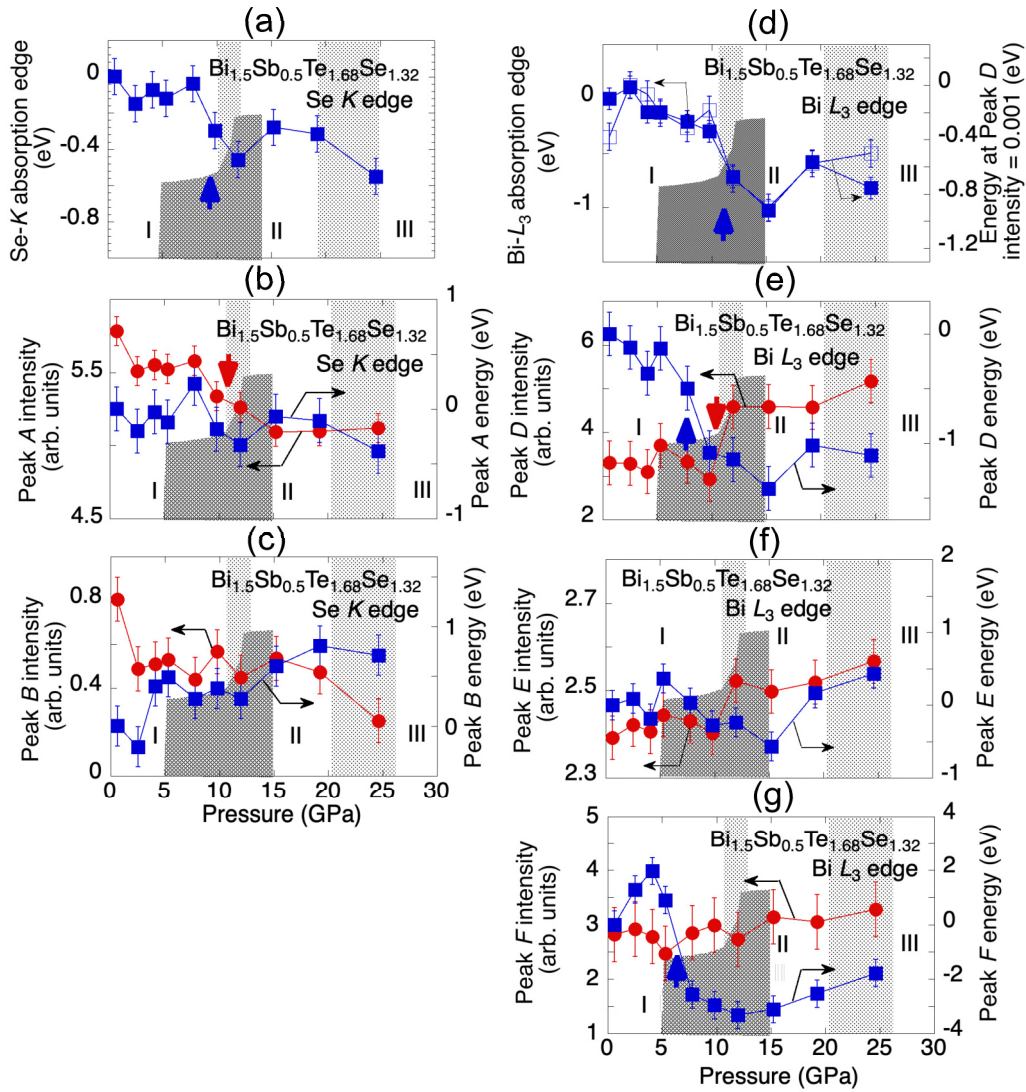


FIG. 3. Analyzed results for $\text{Bi}_{1.5}\text{Sb}_{0.5}\text{Te}_{1.68}\text{Se}_{1.32}$. The measured spectrum is normalized to be 1 by its area. The intensity of each component obtained by the fit is multiplied by a factor of 100. Energy is given relative to the value at the lowest pressure. The two gray areas indicate the boundary regions where two phases coexist, separating the superconducting regions. We also show a pressure dependence of T_c as a dense grey area where the maximum of the vertical axis is scaled to be 8 K [4]. The positions of the large vertical arrows indicate the pressures we refer to in the text. (a) Pressure dependence of the energy of the Se-K absorption edge. [(b),(c)] Pressure dependence of the intensity and energy of the peaks A and B. (d) Pressure dependence of the energy of the Bi- L_3 absorption edge together with the energy at which the intensity of the peak D is 0.001. [(e)–(g)] Pressure dependence of the intensity and energy of the peaks D, E, and F. There are three pressure regions corresponding to the phases I ($R\bar{3}m$), II ($C2/m$), and III (9/10-fold $C2/m$) with different crystal structures [4].

above large change in the electronic structure. But the present results indicate that below P_{s1} , the pressure-induced change in the electronic structure already starts.

The intensity of peak A of Se starts to decrease gradually below P_{s1} , while the intensity of peak D of Bi shows a rapid increase at P_{s1} , which is induced by the structural phase transition, indicating that Bi is more sensitive to the structural phase transition. The energy shifts of the Se-K and Bi- L_3 absorption edges may reflect the change in the energies of the conduction bands and the width of the band gap. In fact, the DFT calculations described below show the lowering of the conduction band and the raising of the valence band with pressure.

The chemical substitution of Sb on the Bi site mainly affects the Bi site as described above, while pressure affects both

Bi and Se sites. But pressure has more effect on the electronic structure of Bi compared to that of Se. The maximum pressure where T_c was measured was 14.2 GPa, which is below the pressure of the second structural phase transition (P_{s2}) [4]. Our results indicate that the change in the electronic structure around P_{s2} is small, which would lead to a prediction of nearly constant T_c for phases II and III in both samples.

C. Pressure dependence of the XAS spectra: $\text{Bi}_{2.1}\text{Te}_{1.8}\text{Se}_{1.2}$

The analyzed results of the $x = 0$ sample are shown in Fig. 4. The measured PFY-XAS spectra are shown in the Supplemental Material [21]. At the Se-K absorption edge, similar to the $x = 0.5$ sample, the energy of the Se-K absorption edge

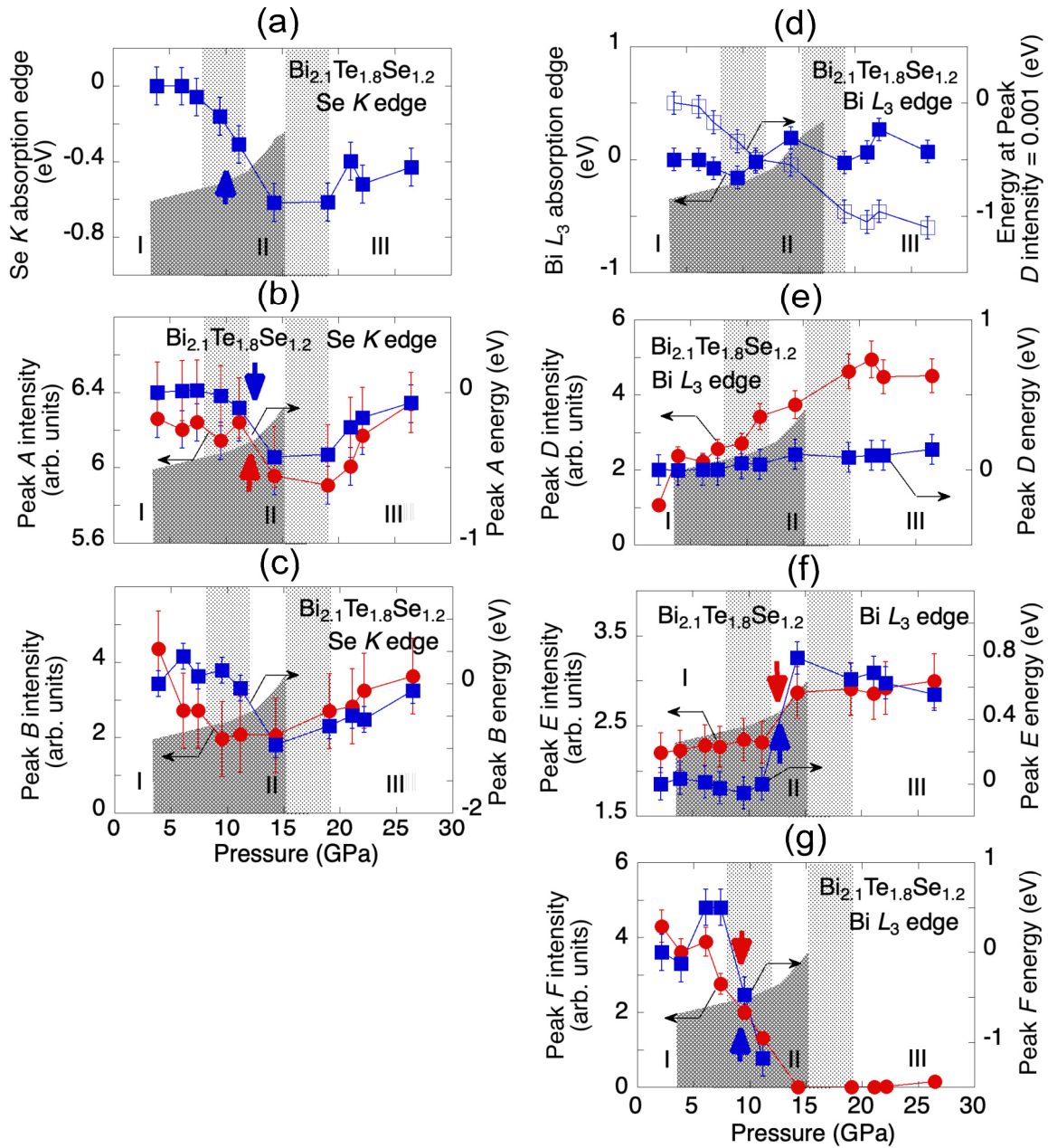


FIG. 4. Analyzed results of $\text{Bi}_{2.1}\text{Te}_{1.8}\text{Se}_{1.2}$. The measured spectrum is normalized to be 1 by its area. The intensity of each component obtained by the fit is multiplied by a factor of 100. Energy is given relative to the value at the lowest pressure. The two gray areas in (a) and (b) indicate the boundary regions where two phases coexist, separating the superconducting regions. We also show a pressure dependence of T_c as a dense grey area where the maximum of the vertical axis is scaled to be 8 K [4]. (a) Pressure dependence of the energy of the Se-K absorption edge. [(b),(c)] Pressure dependence of the intensity and energy of the peaks A and B. (d) Pressure dependence of the energy of the Bi- L_3 absorption edge together with the energy at which the intensity of the peak D is 0.001. [(e)–(g)] Pressure dependence of the intensity and energy of the peaks D, E, and F.

shows a rapid decrease above 5 GPa across the transition from phase I to II as shown in Fig. 4(a). It seems to correlate with the increase of superconducting T_c . The energy and intensity of peak A (Se $4p$ band) show a similar trend with that of the Se-K absorption edge as shown in Fig. 4(b). Figure 4(c) shows that the intensity of the peak B decreases in phase I and increases gradually in phases II and III.

At the Bi- L_3 absorption edge, the energy of the Bi- L_3 absorption edge does not show a clear pressure dependence as shown in Fig. 4(d). The intensity of the peak D (Bi $6s$

band) in Fig. 4(e) increases up to 20 GPa with pressure. The pressure-induced shift of the energy of peak D is not clear, while the energy where peak D has intensity 0.01 decreases monotonically with pressure as shown in Fig. 4(d). This suggests an increase of the unoccupied states of the Bi $6s$ band with pressure similar to the case of $\text{Bi}_{1.5}\text{Sb}_{0.5}\text{Te}_{1.68}\text{Se}_{1.32}$. Figure 4(f) shows that the intensity and energy of the peak E (Bi $6d t_{2g}$ band) shows a rapid increase at pressures between 11.2 and 14.3 GPa, corresponding to the pressure range of the beginning of phase II. The intensity of peak F (Bi $6d e_g$

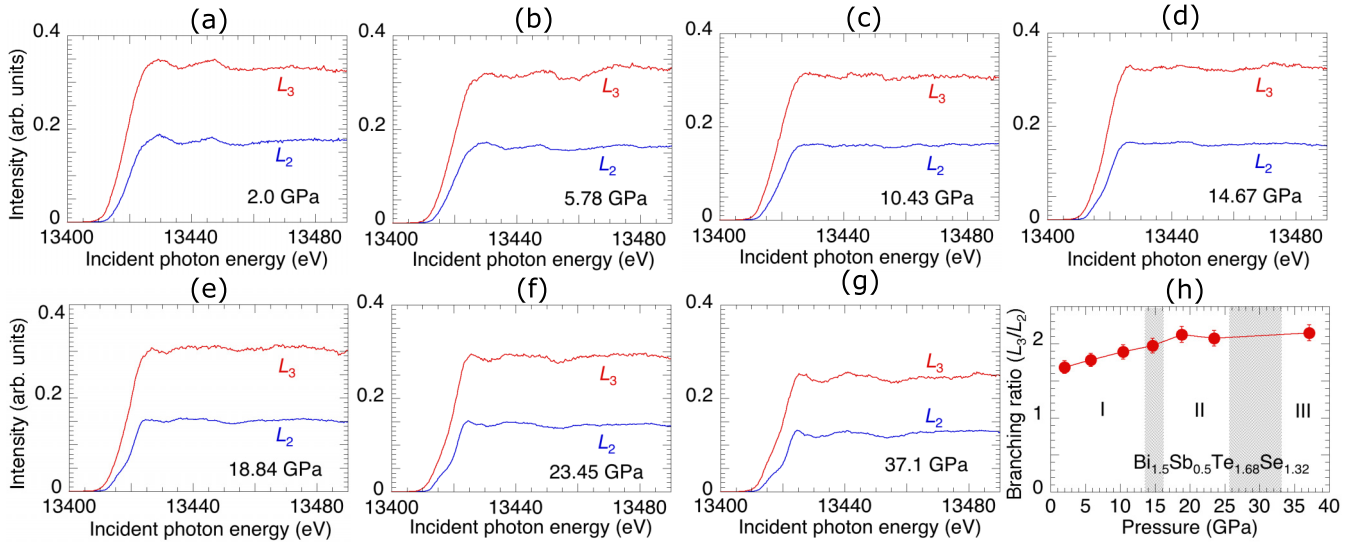


FIG. 5. [(a)–(g)] Pressure dependence of the PFY-XAS spectra of $\text{Bi}_{1.5}\text{Sb}_{0.5}\text{Te}_{1.68}\text{Se}_{1.32}$ at the Bi L_2 and L_3 absorption edges. Note that the incident photon energy at the L_3 absorption edge is shifted by 2300 eV to lower incident energy. (h) Pressure dependence of the intensity ratio of the white peak, the intensity at the L_3 absorption edge divided by that at the L_2 absorption edge, where we define the white peak intensity as a sum of the intensities of the peaks E and F to see the contribution only from the d band. The gray areas in (h) indicate the transition regions separating the superconducting regions

band) in Fig. 4(g) decreases drastically across the transition pressure range from phase I and II and almost disappears above 14 GPa. Thus, the lower Bi $6d$ t_{2g} state is occupied with pressure while the higher Bi $6d$ e_g state is unoccupied rapidly above the transition pressure from phase I to II. These changes in the electronic structure of the Bi $6d$ band are different between $\text{Bi}_{2.1}\text{Te}_{1.8}\text{Se}_{1.2}$ and $\text{Bi}_{1.5}\text{Sb}_{0.5}\text{Te}_{1.68}\text{Se}_{1.32}$. On the other hand, the Se bands did not show such a large change around pressure from P_{s1} to P_{s2} in $\text{Bi}_{2.1}\text{Te}_{1.8}\text{Se}_{1.2}$ as shown in Figs. 4(b) and 4(c). A possible scenario to explain the present results may be that in $\text{Bi}_{2.1}\text{Te}_{1.8}\text{Se}_{1.2}$ the hybridization between the Bi $6d$ and the Te bands becomes larger at P_{s1} compared to the case in $\text{Bi}_{1.5}\text{Sb}_{0.5}\text{Te}_{1.68}\text{Se}_{1.32}$. It is noted that the amount of the Te component has a large effect on the superconducting properties, including the onset pressure of T_c [8,32].

The transition pressure to the superconductor of the $x = 0$ sample is around 4 GPa, which is lower than that of the $x = 0.5$ sample (~ 5 GPa). These pressures are lower than P_{s1} . In our measurements, it is difficult to observe the difference in the electronic structure between the $x = 0$ and 0.5 samples around 4–5 GPa. But we could conclude that in both $x = 0$ and 0.5 samples, the electronic structures start to change below P_{s1} , corresponding to the emergence of superconductivity. Thus, in the $\text{Bi}_{2-x}\text{Sb}_x\text{Te}_{3-y}\text{Se}_y$ systems the first structural transition is not a trigger for the emergence of superconductivity unlike in the $A_x\text{Bi}_2\text{Te}_3\text{Se}_3$ systems, but it does have the effect of raising T_c .

D. XAS spectra at the Bi L_2 and L_3 absorption edges

We also performed measurements of the pressure dependence of PFY-XAS spectra of the $x = 0.5$ sample ($\text{Bi}_{1.5}\text{Sb}_{0.5}\text{Te}_{1.68}\text{Se}_{1.32}$) at the Bi- L_2 and Bi- L_3 absorption edges. The results are shown in Figs. 5(a)–5(g). Note that in

Fig. 5 the incident photon energy at the L_3 absorption edge is shifted by 2300 eV to lower energy.

The electrons in the $2p_{3/2}$ state can be excited to $6s$, $6d_{1/2}$, $6d_{3/2}$, and $6d_{5/2}$ at the Bi- L_3 absorption edge and those in the $2p_{1/2}$ state can be excited to $6s$, $6d_{1/2}$, and $6d_{3/2}$ at the Bi- L_2 absorption edge if there are the unoccupied states. A transition from $2p$ to the $6p$ states is quantum-mechanically forbidden within a dipole approximation.

If we define the Bi white peak as the sum of the peaks of D , E , and F , the white peak is much weaker compared to the case of $5d$ compounds [15]. This may suggest the occupation of $6d$ bands by conduction electrons. It is known that the white line intensity ratio, the branching ratio, at the L_2 to the L_3 edges is calculated to be 2, which is the ratio of the statistical weight of $2J + 1$ of the $2p$ levels. The deviation of the branching ratio to greater than 2 suggests strong spin-orbit interaction [15]. We show the white line intensity ratio in Fig. 5(h), where the contribution from the D component is omitted to see the pure spin-orbit interaction of the d electrons. The branching ratio increases with pressure up to 20 GPa, and a further increase in pressure does not change the ratio. The values of the branching ratio are around 2, indicating nearly no effect of the spin-orbit coupling on the d electrons. It is known that the spin-orbit interaction strongly depends on the angular momentum and the spin-orbit constant of the p orbitals is normally much larger than d orbitals [33,34]. This is a reason why we did not observe the effect of the spin-orbit interaction in this measurement.

IV. ELECTRONIC STRUCTURE CALCULATIONS

We use the structural data determined for the $\text{Bi}_2\text{Te}_2\text{Se}$ and $\text{Bi}_{1.5}\text{Sb}_{0.5}\text{Te}_2\text{Se}$ samples (see Tables in Ref. [21]) to perform electronic structure calculations using the full potential local orbital (FPLO) basis set and a generalized gradient

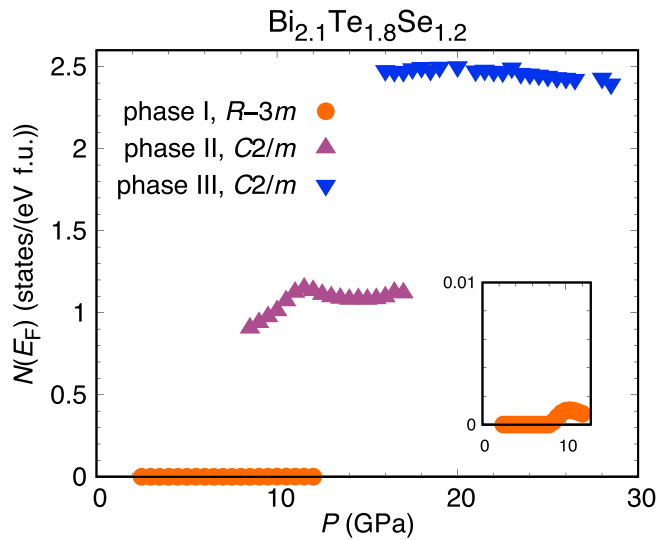


FIG. 6. Density of states at the Fermi level $N(E_F)$ for $\text{Bi}_2\text{Te}_2\text{Se}$ as function of pressure. The inset shows the small metallic $N(E_F)$ in the rhombohedral phase after the closing of the charge gap.

approximation (GGA) to the exchange-correlation functional. We account for the strong spin-orbit coupling in Bi, Sb, Te, and Se by performing fully relativistic DFT calculations. For our calculations, we use the pressure-dependent lattice parameters of $\text{Bi}_2\text{Te}_2\text{Se}$ and $\text{Bi}_{1.5}\text{Sb}_{0.5}\text{Te}_2\text{Se}$ determined in this study. For $\text{Bi}_2\text{Te}_2\text{Se}$, a rhombohedral phase I ($R\bar{3}m$ space group) at ambient pressure is replaced by a monoclinic phase II ($C2/m$ space group) at $P = 8.4$ GPa and by another monoclinic phase III at $P = 15.4$ GPa (so-called 9/10-fold $C2/m$ structure). For $\text{Bi}_{1.5}\text{Sb}_{0.5}\text{Te}_2\text{Se}$, the ambient pressure rhombohedral phase I ($R\bar{3}m$ space group) is replaced by a monoclinic phase II ($C2/m$ space group) at $P = 10.0$ GPa. At $P = 18.7$ GPa, this is replaced by phases III and IV occurring simultaneously. While phase III has a monoclinic $C2/c$ space group, phase IV is a monoclinic $C2/m$ space group. Kim *et al.* also performed the DFT calculations in a wide pressure range for $\text{Bi}_{1.5}\text{Sb}_{0.5}\text{Te}_{1.8}\text{Se}_{1.2}$. But the detailed calculations as a function of pressure were limited to the pressure range of less than 12.09 GPa. Here we performed the detailed pressure dependence of the electronic structure calculations for the three phases of $\text{Bi}_2\text{Te}_2\text{Se}$ and $\text{Bi}_{1.5}\text{Sb}_{0.5}\text{Te}_2\text{Se}$.

The insets in Figs. 6 and 8 indicate that $\text{Bi}_2\text{Te}_2\text{Se}$ and $\text{Bi}_{1.5}\text{Sb}_{0.5}\text{Te}_2\text{Se}$ become metallic around 8 and 7 GPa, respectively, within the rhombohedral phase, so that the results support the experimental observation described above. Figures 6 and 8 also show that monoclinic phases II for both $\text{Bi}_2\text{Te}_2\text{Se}$ and $\text{Bi}_{1.5}\text{Sb}_{0.5}\text{Te}_2\text{Se}$ have substantial density of states at the Fermi level $N(E_F)$; this can explain that superconducting T_c substantially increases within this phase experimentally [4].

Figure 7 shows the pressure-induced insulator to metal transition in the rhombohedral phase I of $\text{Bi}_{1.5}\text{Sb}_{0.5}\text{Te}_2\text{Se}$. The charge gap disappears at around 7 GPa, leading to a small but finite $N(E_F)$. The fact that there still seems to be a tiny indirect band gap at 12 GPa indicates that the L point is not exactly the point with the lowest conduction band energy. The density of states at the Fermi level is even larger in phase III

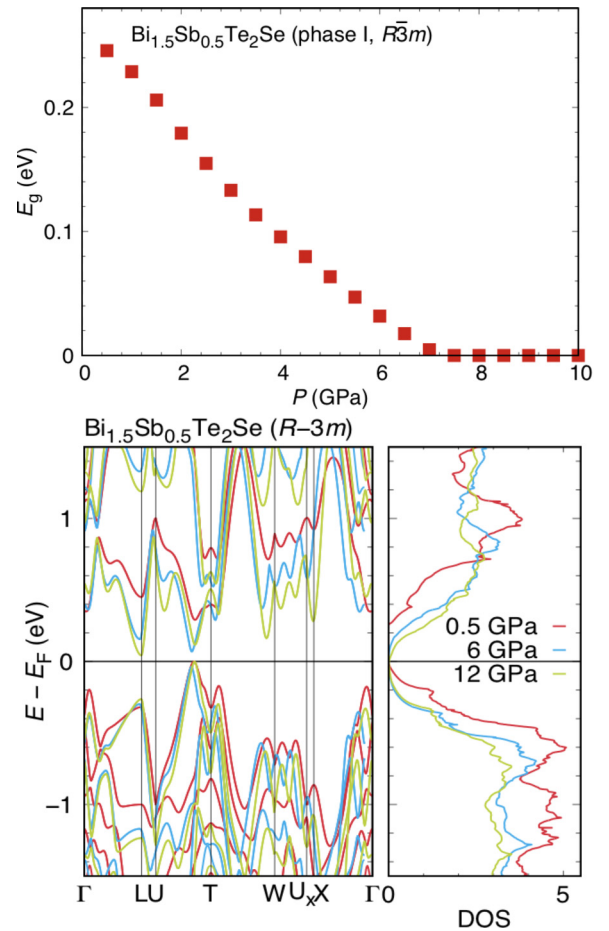


FIG. 7. Charge gap (top) and band structures of $\text{Bi}_{1.5}\text{Sb}_{0.5}\text{Te}_2\text{Se}$ in rhombohedral phase I as function of pressure. At $P = 7$ GPa, the gap disappears as valence and conduction bands touch.

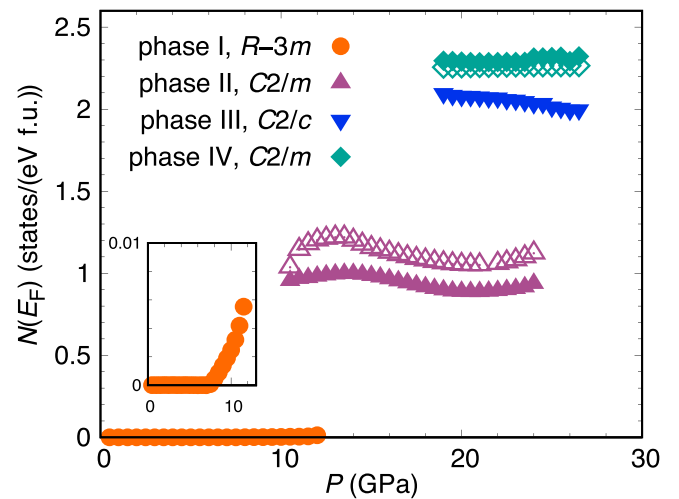


FIG. 8. Density of states at the Fermi level $N(E_F)$ for $\text{Bi}_{1.5}\text{Sb}_{0.5}\text{Te}_2\text{Se}$ as function of pressure. Empty symbols represent calculations with lower symmetry where every fourth Bi is replaced by Sb. The inset shows the small metallic $N(E_F)$ in the rhombohedral phase after the closing of the charge gap.

for $\text{Bi}_2\text{Te}_2\text{Se}$ and in phases III and IV for $\text{Bi}_{1.5}\text{Sb}_{0.5}\text{Te}_2\text{Se}$. Experimentally, the superconducting T_c above 15 GPa was not determined for the present samples [4]. However, the fact that $N(E_F)$ nearly doubles at phase II to phase III transition is in excellent agreement with the substantial T_c increase found in this pressure range in Ref. [47]. Technically, calculations for the $x = 0.5$ compound require the replacement of every fourth Bi by Sb. We did these calculations for phases II and IV (empty symbols in Fig. 8) and find that the results are very similar to calculations for pure Bi in combination with the experimental lattice parameters for $\text{Bi}_{1.5}\text{Sb}_{0.5}\text{Te}_2\text{Se}$ (full symbols in Fig. 8).

Figure 7 also shows that the pressure raises the valence band, lowers the conduction band, and results in the narrowing of the band gap. This is in contrast to the chemical pressure effect where the Sb substitution induced the increase of the band gap although the lattice constants showed a tendency to decrease [3,21].

Figures 3(d) and 3(e) show that both the energies of the Bi- L_3 absorption edge and the peak D start to decrease from around 5 GPa below P_{s1} . These behaviors correspond well to the closing of the band gap in Fig. 7 where the lowest energy of the conduction band shifts toward the Fermi level with pressure.

Experimentally, the intensity of the peaks $E + F$, corresponding to the Bi $6d$ unoccupied states, does not show significant pressure dependencies in $\text{Bi}_{1.5}\text{Sb}_{0.5}\text{Te}_{1.68}\text{Se}_{1.32}$ and $\text{Bi}_{2.1}\text{Te}_{1.8}\text{Se}_{1.2}$ (Fig. S3 in the Supplemental Material [21]). The calculations show approximately 0.4 occupied $6d$ electrons in both phases I and II of $\text{Bi}_{1.5}\text{Sb}_{0.5}\text{Te}_2\text{Se}$, supporting the experimental results.

V. DISCUSSION

In Bi_2Se_3 and $A_x\text{Bi}_2\text{Se}_3$ ($A = \text{Ag}, \text{Sr}$) the pressure-induced first structural phase transition is a trigger of the emergence of superconductivity, where the electronic structure changes significantly [5,6,35–43]. Two different pressure-induced superconducting phases were reported in Bi_2Se_3 , Bi_2Te_3 , $(\text{Bi}, \text{Sb})_2(\text{Se}, \text{Te})_3$, $\text{Bi}_2\text{Te}_2\text{Se}$, and $\text{Bi}_{1.1}\text{Sb}_{0.9}\text{Te}_2\text{S}$ [43–47]. A universal phase diagram was proposed, combing the results of the above materials, where the superconducting regions were divided into low- T_c SC1 and high- T_c SC2 as a function of pressure [47]. In the universal phase diagram, the transition from SC1 to SC2 occurred around the pressure of the structural phase transition from monoclinic ($C2/m$) to tetragonal ($I4/mmm$) phases. They also showed the emergence of the SC1 phase at P_{s1} from the rhombohedral to monoclinic crystal structures.

In $\text{Bi}_{2-x}\text{Sb}_x\text{Te}_{3-y}\text{Se}_y$ superconductivity emerged at a pressure in phase I (rhombohedral structure) below the first phase transition [4]. The present system seems to be an exception to the above universal phase diagram. A question is what the trigger is for the appearance of superconductivity below P_{s1} .

The energy of the peak D of the $x = 0.5$ sample gradually decreases from 5 GPa to 10 GPa, and its intensity increases above 10 GPa suddenly in $\text{Bi}_{1.5}\text{Sb}_{0.5}\text{Te}_{1.68}\text{Se}_{1.32}$. This indicates that the Bi electronic structure starts to change below P_{s1} and shows a large change at that pressure. The results are

correlated to the emergence of the superconductivity below P_{s1} and the sudden increase of T_c above P_{s1} .

In the pressure dependence of the Bi electronic structure, the most crucial evidence is the behavior of the absorption edge and the peak D . The energies of the peak D and the Bi- L_3 absorption edge of the $x = 0.5$ sample gradually decrease from 5 GPa to 10 GPa. The intensity of the peak D increases above P_{s1} suddenly in $\text{Bi}_{1.5}\text{Sb}_{0.5}\text{Te}_{1.68}\text{Se}_{1.32}$ as shown in Figs. 3(d) and 3(e). The shift of the above energies may reflect that of the Fermi level. The decrease of the intensity of the peak D , arising from the $2p$ to $6s$ transition, attributes to the hybridization with other orbitals and also may correspond to the shift of the above energies, which could be closely connected to the narrowing of the band gap. Thus, the electronic structure starts to change below P_{s1} and it changes strongly around the structural transition pressure with the rapid enhancement of T_c . Our calculated results for $\text{Bi}_2\text{Te}_2\text{Se}$ and $\text{Bi}_{1.5}\text{Sb}_{0.5}\text{Te}_2\text{Se}$ in Fig. 7 support the experimental results that the band gap closes around 8 and 7 GPa, and DOS at the Fermi level start to increase within the rhombohedral phase, respectively, which could be a trigger of the emergence of the superconductivity. The sudden enhancement of the DOS at the Fermi level around 10 GPa in $\text{Bi}_{1.5}\text{Sb}_{0.5}\text{Te}_2\text{Se}$ connected to the increase of T_c caused by the structural phase transition.

On the other hand, the change in the electronic structure and the enhancement of T_c in $\text{Bi}_2\text{Te}_2\text{Se}$ are more gradual compared to the case of $\text{Bi}_{1.5}\text{Sb}_{0.5}\text{Te}_2\text{Se}$ around the pressure range from Phase I to II. This may be due to the wider pressure range of the boundary where two phases coexist in $\text{Bi}_2\text{Te}_2\text{Se}$. A similar calculated results for $\text{Bi}_{1.5}\text{Sb}_{0.5}\text{Te}_{1.8}\text{Se}_{1.2}$ were reported by Kim *et al.* [7] They suggested the non-trivial state at phase I and a trivial semimetal state at 12.1 GPa. On the other hand, in our calculations, Z_2 invariant calculated for each crystal phase of $\text{Bi}_2\text{Te}_2\text{Se}$ under pressure indicated a strong topological nature at phase I, a topologically trivial nature at phase II, and a strong topological nature at phase III. The band gap disappeared in phases II and III. However, the Z_2 invariant for phase II was very sensitive to the crystal structure, and the topologically trivial nature was still under discussion [4].

VI. CONCLUSIONS

In this study, we investigate the correlation between electronic structure and the emergence of superconductivity by the measurements of the electronic structure and by DFT calculations. We measured the x dependence of the PFY-XAS spectra of $\text{Bi}_{2-x}\text{Sb}_x\text{Te}_{3-y}\text{Se}_y$ ($x = 0, 0.25, 0.5, 1.0$, and $y \sim 1.2$) at the Se- K and Bi- L_3 absorption edges. The chemical substitution of Sb to the Bi site mainly affects the Bi site. We found a downward shift of the energy of the Bi- L_3 absorption edge by 0.3 eV between $x = 0$ and 1.0, which may suggest a change in the Bi charge state.

We also measured the pressure dependence of the PFY-XAS spectra for the $x = 0.5$ and 0 samples ($\text{Bi}_{1.5}\text{Sb}_{0.5}\text{Te}_{1.68}\text{Se}_{1.32}$ and $\text{Bi}_{2.1}\text{Te}_{1.8}\text{Se}_{1.2}$). Common features were observed for both samples. The pressure affects both the Bi and Se sites. The shifts of the Se- K and Bi- L_3 absorption edges may correspond to the increase in the unoccupied states of the Bi $6s$ and $6d$ t_{2g} bands, suggesting the increase of the hybridization with pressure. These electronic structure

changes may correlate to the emergence of the superconductivity at pressures below P_{s1} . The first structural transition enhanced T_c rapidly with changing the electronic structure significantly in $\text{Bi}_{1.5}\text{Sb}_{0.5}\text{Te}_{1.68}\text{Se}_{1.32}$. The experimental observations are supported by the detailed DFT calculations as a function of pressure for $\text{Bi}_2\text{Te}_2\text{Se}$ and $\text{Bi}_{1.5}\text{Sb}_{0.5}\text{Te}_2\text{Se}$. The calculations showed the closing of the gap and increasing DOS at the Fermi level at the pressures below P_{s1} .

The pressure dependence of T_c above the pressure around the second phase transition has been measured in Ref. [47] but not in Ref. [4] for the samples measured in this paper. Our electronic structure calculations are in excellent agreement with superconducting T_c being nearly constant within phase II and within phase III but being substantially larger for the second superconducting phase; both these observations are borne out by the densities of states at the Fermi level we find in extensive calculations for both $x = 0$ and $x = 0.5$ structures of $\text{Bi}_{2-x}\text{Sb}_x\text{Te}_{3-y}\text{Se}_y$. From our measurements, we do not

find a substantial change in the electronic structure above around P_{s2} .

ACKNOWLEDGMENTS

The experiments were performed at SPring-8 Taiwan beamline BL12XU under SPring-8 Proposals No. 2018A4257, No. 2019A4266, No. 2019B4269, No. 2021B4254, and No. 2022A4258, corresponding NSRRC Proposals No. 2018-2-010, No. 2019-2-030, No. 2019-3-004, No. 2021-1-009, and No. 2022-2-104. We thank Kagehisa Takai, and Yanan Wang at Okayama University for their help in the experiments. We also appreciate Jun'ichiro Mizuki at Kwansai-Gakuin University for his useful comments. This work has been partly supported by Grants-in-Aid for Scientific Research (KAKENHI 18K18743, 20H05878, and 20H05879) from MEXT, Japan, and by the Program for Promoting the Enhancement of Research Universities.

-
- [1] M. Z. Hasan and C. L. Kane, Colloquium: Topological insulators, *Rev. Mod. Phys.* **82**, 3045 (2010).
- [2] Z. Ren, A. A. Taskin, S. Sasaki, K. Segawa, and Y. Ando, Optimizing $\text{Bi}_{2-x}\text{Sb}_x\text{Te}_{3-y}\text{Se}_y$ solid solutions to approach the intrinsic topological insulator regime, *Phys. Rev. B* **84**, 165311 (2011).
- [3] T. Arakane, T. Sato, S. Souma, K. Kosaka, K. Nakayama, M. Komatsu, T. Takahashi, Z. Ren, K. Segawa, and Y. Ando, Tunable Dirac cone in the topological insulator $\text{Bi}_{2-x}\text{Sb}_x\text{Te}_{3-y}\text{Se}_y$, *Nat. Commun.* **3**, 636 (2012).
- [4] T. He, X. Yang, T. Taguchi, T. Ueno, K. Kobayashi, J. Akimitsu, H. Yamaoka, H. Ishii, Y.-F. Liao, H. Ota, H. Goto, R. Eguchi, K. Terashima, T. Yokoyama, and Y. Kubozono, Pressure-induced superconductivity in $\text{Bi}_{2-x}\text{Sb}_x\text{Te}_{3-y}\text{Se}_y$, *Phys. Rev. B* **100**, 094525 (2019).
- [5] T. He, X. F. Yang, T. Terao, T. Uchiyama, T. Ueno, K. Kobayashi, J. Akimitsu, T. Miyazaki, T. Nishioka, K. Kimura, K. Hayashi, N. Hoppo, H. Yamaoka, H. Ishii, Y.-F. Liao, H. Ota, and Y. Kubozono, Pressure-induced superconductivity in $\text{Ag}_x\text{Bi}_{2-x}\text{Se}_3$, *Phys. Rev. B* **97**, 104503 (2018).
- [6] H. Yamaoka, H. O. Jeschke, X. Yang, T. He, H. Goto, N. Hiraoka, H. Ishii, J. Mizuki, and Y. Kubozono, Electronic structures of Bi_2Se_3 and $\text{Ag}_x\text{Bi}_2\text{Se}_3$ under pressure studied by high-resolution x-ray absorption spectroscopy and density functional theory calculations, *Phys. Rev. B* **102**, 155118 (2020).
- [7] J.-S. Kim, R. Juneja, N. P. Salke, W. Palosz, V. Swaminathan, S. Trivedi, A. K. Singh, D. Akinwande, and J.-Fu Lin, Structural, vibrational, and electronic topological transitions of $\text{Bi}_{1.5}\text{Sb}_{0.5}\text{Te}_{1.8}\text{Se}_{1.2}$ under pressure, *J. Appl. Phys.* **123**, 115903 (2018).
- [8] T. He, X. Yang, T. Taguchi, L. Zhi, T. Miyazaki, K. Kobayashi, J. Akimitsu, H. Ishii, Y.-F. Liao, H. Goto *et al.*, Superconductivity in $\text{Bi}_{2-x}\text{Sb}_x\text{Te}_{3-y}\text{Se}_y$ ($x = 1.0$ and $y = 2.0$) under pressure, *J. Phys.: Condens. Matter* **32**, 465702 (2020).
- [9] K. Hämäläinen, D. P. Siddons, J. B. Hastings, and L. E. Berman, Elimination of the Inner-Shell Lifetime Broadening in X-Ray-Absorption Spectroscopy, *Phys. Rev. Lett.* **67**, 2850 (1991).
- [10] K. Hämäläinen, C. C. Kao, J. B. Hastings, D. P. Siddons, L. E. Berman, V. Stojanoff, and S. P. Cramer, Spin-dependent x-ray absorption of MnO and MnF_2 , *Phys. Rev. B* **46**, 14274 (1992).
- [11] J.-P. Rueff and A. Shukla, Inelastic x-ray scattering by electronic excitations under high pressure, *Rev. Mod. Phys.* **82**, 847 (2010).
- [12] H. Yamaoka, Pressure dependence of the electronic structure of $4f$ and $3d$ electron systems studied by x-ray emission spectroscopy, *High Press. Res.* **36**, 262 (2016).
- [13] H. Yamaoka, Y. Yamamoto, E. F. Schwier, N. Tsujii, M. Yoshida, Y. Ohta, H. Sakurai, J.-F. Lin, N. Hiraoka, H. Ishii, K.-D. Tsuei, M. Arita, K. Shimada, and J. Mizuki, Pressure-induced phase transition in LaCo_5 studied by x-ray emission spectroscopy, x-ray diffraction and density functional theory, *Phys. Rev. B* **94**, 165156 (2016).
- [14] H. Yamaoka, Y. Yamamoto, J.-F. Lin, Junjie J. Wu, X. Wang, C. Jin, M. Yoshida, S. Onari, S. Ishida, Y. Tsuchiya, N. Takeshita, N. Hiraoka, H. Ishii, K.-D. Tsuei, P. Chow, Y. Xiao, and J. Mizuki, Electronic structures and spin states of BaFe_2As_2 and SrFe_2As_2 probed by x-ray emission spectroscopy at Fe and As K -absorption edges, *Phys. Rev. B* **96**, 085129 (2017).
- [15] J. P. Clancy, N. Chen, C. Y. Kim, W. F. Chen, K. W. Plumb, B. C. Jeon, T. W. Noh, and Young-June Kim, Spin-orbit coupling in iridium-based $5d$ compounds probed by x-ray absorption spectroscopy, *Phys. Rev. B* **86**, 195131 (2012).
- [16] H.-K. Mao and P. M. Bell, High-pressure physics: The 1-megabar mark on the ruby $R1$ static pressure scale, *Science* **191**, 851 (1976).
- [17] K. Syassen, Ruby under Pressure, *High Press. Res.* **28**, 75 (2008).
- [18] H. Yamaoka, Y. Zekko, I. Jarrige, J.-F. Lin, N. Hiraoka, H. Ishii, K.-D. Tsuei, and J. Mizuki, Ruby pressure scale in a

- low-temperature diamond anvil cell, *J. Appl. Phys.* **112**, 124503 (2012).
- [19] K. Koepnick and H. Eschrig, Full-potential nonorthogonal local-orbital minimum-basis band-structure scheme, *Phys. Rev. B* **59**, 1743 (1999); <http://www.FPLO.de>.
- [20] J. P. Perdew, K. Burke, and M. Ernzerhof, Generalized Gradient Approximation Made Simple, *Phys. Rev. Lett.* **77**, 3865 (1996).
- [21] See Supplemental Material <http://link.aps.org/supplemental/10.1103/PhysRevB.108.035146> for additional results of the PFY-XAS spectra of the $x = 0$ sample at the Se- K and Bi- L_3 absorption edges, the pressure dependence of the Bi d states, the pressure dependence of T_c and volume, lattice constant, and ratio c/a are shown. We also show the pressure evolution of the total density of states of $\text{Bi}_2\text{Te}_2\text{Se}$ in the three phases and the density of states at the Fermi level $N(E_F)$ and $sN(E_F)$ for $\text{Bi}_2\text{Te}_2\text{Se}$. It includes Refs. [2], [4], and [46–49].
- [22] B. Joseph, A. Iadecola, L. Simonelli, Y. Mizuguchi, Y. Takano, T. Mizokawa, and N. L. Saini, A study of the electronic structure of $\text{FeSe}_{1-x}\text{Te}_x$ chalcogenides by Fe and Se K -edge x-ray absorption near edge structure measurements, *J. Phys.: Condens. Matter* **22**, 485702 (2010).
- [23] C. L. Chen, S. M. Rao, C. L. Dong, J. L. Chen, T. W. Huang, B. H. Mok, M. C. Ling, W. C. Wang, C. L. Chang, and T. S. Chan, X-ray absorption spectroscopy investigation of the electronic structure of superconducting FeSe_x single crystals, *Europhys. Lett.* **93**, 47003 (2011).
- [24] N. L. Saini, T. Mizokawa, E. Magnano, S. Nappini, F. Bondino, H. Takeya, Y. Mizuguchi, Y. Takano, and K. B. Garg, X-ray absorption and photoemission spectroscopy of electronic phase separation in $\text{K}_x\text{Fe}_{2-y}\text{Se}_2$, *Phys. Rev. B* **90**, 184510 (2014).
- [25] A. I. Figueroa, G. der Laan, L. J. Collins-McIntyre, G. Cibin, A. J. Dent, and T. Hesjedal, Local structure and bonding of transition metal dopants in Bi_2Se_3 topological insulator thin films, *J. Phys. Chem.* **119**, 17344 (2015).
- [26] A. A. Rahman, R. Huang, and L. Whittaker-Brooks, Distinctive extrinsic atom effects on the structural, optical, and electronic properties of $\text{Bi}_2\text{S}_{3-x}\text{Se}_x$ Solid Solutions, *Chem. Mater.* **28**, 6544 (2016).
- [27] A. N. Baranov, J. S. Kim, D. C. Kim, D. S. Suh, Y. W. Park, and E. V. Antipov, X-ray absorption near-edge structure spectra study of the $\text{Ba}_{1-x}\text{K}_x\text{BiO}_3$ ($0.37 \leq x \leq 1.0$) superconductor, *Physica C* **383**, 95 (2002).
- [28] Q. Zhou, P. E. R. Blanchard, B. J. Kennedy, C. D. Ling, S. Liu, M. Avdeev, J. B. Aitken, A. Tadich, and H. E. A. Brand, Diffraction and spectroscopic study of pyrochlores $\text{Bi}_{2-x}\text{Fe}_{1+x}\text{SbO}_7$, *J. Alloys Compd.* **589**, 425 (2014).
- [29] N. Jiang and J. C. H. Spence, Can near-edge structure of the Bi L_3 edge determine the formal valence states of Bi, *J. Phys.: Condens. Matter* **18**, 8029 (2006).
- [30] S. M. Heald, D. DiMarzio, M. Croft, M. S. Hegde, S. Li, and M. Greenblatt, X-ray-absorption study of charge-density ordering in $(\text{Ba}_{1-x}\text{K}_x)\text{BiO}_3$, *Phys. Rev. B* **40**, 8828 (1989).
- [31] R. Retoux, F. Studer, C. Michel, B. Raveau, A. Fontaine, and E. Dartyge, Valence state for bismuth in the superconducting bismuth cuprates, *Phys. Rev. B* **41**, 193 (1990).
- [32] J. L. Zhang, S. J. Zhang, H. M. Weng, W. Zhang, L. X. Yang, Q. Q. Liu, S. M. Feng, X. C. Wang, R. C. Yu, L. Z. Cao *et al.*, Pressure-induced superconductivity in topological parent compound Bi_2Te_3 , *Proc. Natl. Acad. Sci. USA* **108**, 24 (2011).
- [33] M. Vijayakumar and M. S. Gopinathan, Spin-orbit coupling constants of transition metal atoms and ions in density functional theory, *J. Mol. Struct.: THEOCHEM* **361**, 15 (1996).
- [34] H. Haken and H. C. Wolf, *The Physics of Atoms and Quanta: Introduction to Experiments and Theory*, 7th ed. (Springer, New York, 2005).
- [35] P. P. Kong, J. L. Zhang, S. J. Zhang, J. Zhu, Q. Q. Liu, R. C. Yu, Z. Fang, C. Q. Jin, W. G. Yang, X. H. Yu, J. L. Zhu, and Y. S. Zhao, Superconductivity of the topological insulator Bi_2Se_3 at high pressure, *J. Phys.: Condens. Matter* **25**, 362204 (2013).
- [36] Z. Yu, L. Wang, Q. Hu, J. Zhao, S. Yan, K. Yang, S. Sinogeikin, G. Gu, and H.-k. Mao, Structural phase transitions in Bi_2Se_3 under high pressure, *Sci. Rep.* **5**, 15939 (2015).
- [37] A. M. Nikitin, Y. Pan, Y. K. Huang, T. Naka, and A. de Visser, High-pressure study of the basal-plane anisotropy of the upper critical field of the topological superconductor $\text{Sr}_x\text{Bi}_2\text{Se}_3$, *Phys. Rev. B* **94**, 144516 (2016).
- [38] T. V. Bay, T. Naka, Y. K. Huang, H. Luigjes, M. S. Golden, and A. de Visser, Superconductivity in the Doped Topological Insulator $\text{Cu}_x\text{Bi}_2\text{Se}_3$ under High Pressure, *Phys. Rev. Lett.* **108**, 057001 (2012).
- [39] Y. S. Hor, A. J. Williams, J. G. Checkelsky, P. Roushan, J. Seo, Q. Xu, H. W. Zandbergen, A. Yazdani, N. P. Ong, and R. J. Cava, Superconductivity in $\text{Cu}_x\text{Bi}_2\text{Se}_3$ and its Implications for Pairing in the Undoped Topological Insulator, *Phys. Rev. Lett.* **104**, 057001 (2010).
- [40] K. Manikandan, Shruti, P. Neha, G. Kalai Selvan, B. Wang, Y. Uwatoko, K. Ishigaki, R. Jha, V. P. S. Awana, and S. Arumugam, Possibility for conventional superconductivity in $\text{Sr}_{0.1}\text{Bi}_2\text{Se}_3$ from high-pressure transport studies, *Europhys. Lett.* **118**, 47008 (2017).
- [41] Y. H. Zhou, X. L. Chen, R. R. Zhang, J. F. Shao, X. F. Wang, C. An, Y. Zhou, C. Y. Park, W. Tong, L. Pi, Z. R. Yang, C. J. Zhang, and Y. H. Zhang, Pressure-induced reemergence of superconductivity in topological insulator $\text{Sr}_{0.065}\text{Bi}_2\text{Se}_3$, *Phys. Rev. B* **93**, 144514 (2016).
- [42] Z. Liu, X. Yao, J. Shao, M. Zuo, L. Pi, S. Tan, C. Zhang, and Y. Zhang, Superconductivity with topological surface state in $\text{Sr}_x\text{Bi}_2\text{Se}_3$, *J. Am. Chem. Soc.* **137**, 10512 (2015).
- [43] K. Kirshenbaum, P. S. Syers, A. P. Hope, N. P. Butch, J. R. Jeffries, S. T. Weir, J. J. Hamlin, M. B. Maple, Y. K. Vohra, and J. Paglione, Pressure-Induced Unconventional Superconducting Phase in the Topological Insulator Bi_2Se_3 , *Phys. Rev. Lett.* **111**, 087001 (2013).
- [44] K. Matsubayashi, T. Terai, J. S. Zhou, and Y. Uwatoko, Superconductivity in the topological insulator Bi_2Se_3 under hydrostatic pressure, *Phys. Rev. B* **90**, 125126 (2014).
- [45] C. Zhang, L. Sun, Z. Chen, X. Zhou, Q. Wu, W. Yi, J. Guo, X. Dong, and Z. Zhao, Phase diagram of a pressure-induced superconducting state and its relation to the Hall coefficient of Bi_2Te_3 single crystals, *Phys. Rev. B* **83**, 140504(R) (2011).
- [46] J. R. Jeffries, N. P. Butch, Y. K. Vohra, and S. T. Weir, Pressure evolution of electrical transport in the 3D topological

- insulator $(\text{Bi, Sb})_2(\text{Se, Te})_3$, *J. Phys.: Conf. Ser.* **592**, 012124 (2015).
- [47] S. Cai, S. K. Kushwaha, J. Guo, V. A. Sidorov, C. Le, Y. Zhou, H. Wang, G. Lin, X. Li, Y. Li, K. Yang, A. Li, Q. Wu, J. Hu, R. J. Cava, and L. Sun, Universal superconductivity phase diagram for pressurized tetradymite topological insulators, *Phys. Rev. Mater.* **2**, 114203 (2018).
- [48] I. V. Zhevstovskikh, Y. S. Ponosov, S. G. Titova, N. S. Averkiev, V. V. Gudkov, M. N. Sarychev, T. V. Kuznetsova, K. A. Kokh, and O. E. Tereshchenko, Anomalous behavior of the elastic and optical properties in $\text{Bi}_{1.5}\text{Sb}_{0.5}\text{Te}_{1.8}\text{Se}_{1.2}$ topological insulator induced by point defects, *Phys. Status Solidi B* **255**, 1800264 (2018).
- [49] T. He, Pressure-driven superconductivity in topological insulators, Ph.D. thesis, Okayama University, 2019.